Heliyon 9 (2023) e18011

Contents lists available at ScienceDirect

Heliyon

journal homepage: www.cell.com/heliyon

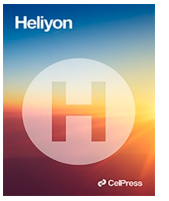

Lumican is a potential predictor on the efficacy of concurrent chemoradiotherapy in cervical squamous cell carcinoma

Ge Hu [a,1], Ying Xiao [b,1], Chanchan Ma [c,1], Jinyun Wang [a], Xiaotao Qian [a], Xiaowei Wu [a], Fengqin Zhu [a], Shiying Sun [c,**], Junchao Qian [a,*]

[a] *Hefei Cancer Hospital, Chinese Academy of Sciences, Hefei,230031, PR China*
[b] *The Affiliated Jiangning Hospital of Nanjing Medical University, Nanjing 211100, PR China*
[c] *Department of Obstetrics and Gynecology, Second Affiliated Hospital of Anhui Medical University, Hefei, 230031, PR China*

ARTICLE INFO

Keywords:
CESC
LUM
CCRT
Biomarker

ABSTRACT

Purpose: To identify new novel biomarkers for predicting the efficacy of concurrent chemoradiotherapy(CCRT) in cervical squamous cell carcinoma(CESC).
Methods: Gene expression datasets GSE56363, GSE5787, and GSE168009 were analyzed to identify candidate genes to predict the efficacy of CCRT in CESC. Single-cell RNA sequencing (scRNA-seq) data from GSE168652 and CESC patients in The Cancer Genome Atlas(TCGA) were systematically analyzed to explore possible molecular mechanisms. Kaplan-Meier evaluated the correlation between LUM (Lumican) and prognostic significance. The expression of LUM protein in biopsy tissues before CCRT was detected by immunohistochemistry in 15 CESC patients.
Results: LUM mRNA levels were significantly upregulated in nonresponders of CESC.
patients receiving CCRT and positively correlated with poor therapeutic effect. Furthermore, high expression of LUM influenced the immune microenvironment in CESC patient-derived organoids treated with CCRT. LUM overexpression in CESC cells induced resistance to CCRT, potentially via immune landscape modulation. Gene Set Enrichment Analysis (GSEA) revealed that possible mechanisms underlying resistance to CCRT might involve the PARs and IL1 signaling pathway affecting the immune landscape.
Conclusions: High LUM expression is correlated with poor efficacy in CESC patients receiving CCRT, possibly through the PARs and IL1 signaling pathway affecting the immune landscape.

1. Introduction

Cervical cancer ranks fourth in morbidity and mortality among women worldwide, following breast, colorectal, and lung cancer [1, 2]. According to the International Agency for Research on Cancer (IARC), in 2020, approximately 604,000 women were diagnosed with cervical cancer, and about 342,000 women died from the disease worldwide [3]. Persistent infection with high-risk human papillomavirus (HPV), a widespread family of viruses spread through sexual contact, is the leading cause of cervical cancer [4]. Although vaccines can prevent high-risk HPV types and screening programs can detect early signs of disease for effective treatment and

* Corresponding author.
** Corresponding author.
E-mail addresses: sunsy71@hotmail.com (S. Sun), qianjunchao@hmfl.ac.cn (J. Qian).
[1] These authors contributed to the work equally and should be regarded as co-first authors.

https://doi.org/10.1016/j.heliyon.2023.e18011
Received 16 February 2023; Received in revised form 25 June 2023; Accepted 5 July 2023
Available online 8 July 2023

management, these measures are more common in high-income countries. In developing countries, the incidence and mortality from cervical cancer remain high [4,5]. This suggests that cervical cancer should be one of the most preventable and treatable forms of cancer. China significantly contributors to the global cervical cancer burden due to differences in population size, geographic location, and economic conditions, especially in central and western China and rural areas. Prevention and control measures, including HPV vaccination and screening programs, require strengthening based on local conditions [5–7].

In China, the most prevalent type of cervical cancer is cervical squamous cell carcinoma (CESC). Most patients are locally advanced at the time of diagnosed, and concurrent chemoradiotherapy (CCRT) is the standard mode of treatment for these patients [8–10]. However, the 5-year-overall survival (OS) of locally advanced cervical cancer remains at approximately 40%, and the 3-year disease-free survival (DFS) rate ranges from 65 to 75% [10,11]. Therapy resistance in a subset of patients presents a major clinical challenge; 8 to 26% of women with cervical cancer experience relapse of disease, typically within the first two years of completing primary treatment, and fewer than 5% of them remain alive five years after recurrence [12–14]. Therefore, predicting the treatment efficacy of cervical cancer patients receiving CCRT in advance is essential. A personalized treatment plan can be developed based on the expected results before initiating treatment to enhance treatment efficacy. Thus, identifying a reliable method to predict the prognosis of patients with cervical cancer receiving CCRT is crucial.

LUM (Lumican) is a member of the small leucine-rich proteoglycans family, located on chromosome 12q21.3-q22 [15,16]. LUM is predominantly expressed in connective tissues and participates in tissue reconstruction [16–18]. Recent studies have demonstrated that LUM is involved in various tumor-related cellular processes such as epithelial-mesenchymal transformation, cell proliferation, migration, invasion, and adhesion [19,20]. Li et al. [21] discovered that extracellular LUM enhances chemotherapy cytotoxicity in PDAC cells through reduced AMPK activity and inhibition of chemotherapeutic agent-induced autophagy. Nizet et al. [22] showed that LUM primarily inhibits ovarian cancer growth by altering collagen fibrillogenesis. LUM expression differs among tumors and is reported as a reference for tumor prognosis, but its association with tumor progression and treatment resistance varies across tumors [22–24]. No studies have examined the efficacy of LUM and CCRT in CESC.

In this study, we analyzed RNA arrays, single-cell RNA-seq and bulk RNA-seq from the GEO (Gene Expression Omnibus) database, along with bulk RNA-seq from TCGA databases. Our results indicated that high LUM expression correlates with poor efficacy in CESC patients receiving CCRT, potentially through the PARs and IL1 signaling pathways affecting the immune landscape.

2. Materials and methods

2.1. Data source and differential genes (DEGs) analysis

RNA microarray GSE56363, GSE5787, bulk RNA-seq GSE168009 data, and single-cell RNA-seq data of CESC patients were obtained from the GEO database (www.ncbi.nlm.nih.gov/geo). In GSE56363 and GSE5787, patients were divided into two groups according to the patient's clinical response: complete response to CCRT (CR) and non-complete response to CCRT (NCR). In GSE168009, patients were divided into two groups according to the patient' durable benefit: no durable benefit (NDB) and durable clinical benefit (DCB). The DEGs were analyzed using the limma package in R. False discovery rate (FDR) < 0.05 and $|\log2\text{foldchange (Log2FC)}| \geq 1$ were considered the cut-off criterion.

2.2. Construction the protein-protein Interaction(PPI) network and identifying hub genes

The STRING website (https://string-db.org/) was used to reveals the PPI of DEGs and Cytoscape3.7.2 was employed for network visualization. The PPI network was then analyzed with the cytoHubba plugin, and the top 10 hub DEGs with the highest degrees were selected for further analysis. GO (Gene Ontology) enrichment for the top 10 DEGs related to CCRT resistance in CESC was performed using the ClueGO v2.5.8 and CluePedia v1.5.8 plugins. The MCODE PPI and enrichment analysis of LUM DEGs in single-cell RNA data were conducted using Metascape (http://metascape.org).

2.3. Single-cell data analysis

The Seurat v4 (version 4.0.4) R package was used to analyze the scRNA-seq data. The annotation of significant cell types was performed according to the original article, and the annotation of cell subtypes was conducted based on their highly expressed marker genes or well-known functional genes. First, we normalize the merged data through log-normalization and find the first 2000 highly variable genes through the Find Variable Features function (based on the variable features, ("vst")). Simultaneously, all genes were scaled using the ScaleData function, and RunPCA function was applied to reduce the dimension of PCA for the first 2000 highly variable genes screened above. We chose dim = 20 and clustered the cells using the "FindNeighbors" and "FindClusters" functions (resolution = 0.5) to determine the cell clusters. Finally, the FindAllMarkers part was used to screen the marker genes of subgroups with Log2FC = 0.6 (differential multiples), Minpct = 0.4 (the expression ratio of the minor differential genes), and a corrected $p <$ 0.05. After identifying the cell types in scRNA-seq, R package Cell Chat was utilized to analyze cell subsets communication in the tumor group. The Nebulosa (v1.6.0) package was employed to perform gene expression using the plot_density function with default parameters.

2.4. Tumour immune dysfunction and exclusion (TIDE)

Potential Immune checkpoint blockade (ICB) response and TIDE score were predicted with the TIDE algorithm. The combined array from GSE56363, GSE5787, and the RNA-seq from the TCGA database was grouped by LUM expression (highest 25% compared with lowest 25%).

2.5. Immunomodulation analysis

CIBERSORT and TIMER algorithms were employed to investigate the immune cells in high-level LUM and low-level LUM samples (comparing the highest 25% with the lowest 25%). The CESC TMB scores were obtained from TCGA, and the correlation analysis with LUM expression was conducted using Spearman analysis. Immune checkpoint gene levels were compared between high-level LUM and low-level LUM samples (highest 25% compared with the lowest 25%). The ESTIMATE algorithm was utilized to calculate the Estimate Score. $p < 0.05$ indicated statistical significance.

2.6. Survival analysis using Kaplan-Meier plotter

Kaplan-Meier plots were obtained from the KM plot database(http://www.kmplot.com/analysis). The significant difference in survival analysis was defined as $p < 0.05$.

2.7. Gene set enrichment analysis (GSEA)

CR patients in the merged GSE56363 and GSE5787 were classified into the high and low LUM expression groups (50% cut off) and then analyzed with GSEA (version 3.0). GSEA utilized default weighted enrichment statistics with 1,000 random combinations. The calculating criteria of $p < 0.05$, normalized enrichment score (NES) of >1.3, and (FDR) of <25% were considered significant.

2.8. Gene set variation analysis (GSVA)

The GSVA scores for single-cell RNA data were calculated using the R package GSVA, and the cell matrix was averaged based on clusters employing the AverageExpression function from the Seurat package.

2.9. Tissue immunohistochemistry (IHC)

The Medical Ethics Committee of Hefei Cancer Hospital, Chinese Academy of Sciences approved this study. All patients had been informed that their tissue samples would be used for diagnosis and scientific research for clinical treatment at the hospital. This study complies with the Declaration of Helsinki. 15 CESC tissue specimens were collected between March 2018 and December 2021. All patients were diagnosed with CESC and had not received treatment with chemotherapy, radiotherapy, or immunotherapy before the biopsy.

IHC was performed on serial paraffin sections using an EnVision kit (Dako). Antigens were retrieved using citrate pH 6.0 buffer. Endogenous peroxidase was blocked by pre-incubation in a solution of 3% H_2O_2, performed in 1x phosphate-buffered saline with 10% goat serum. Slides were incubated overnight at 4 °C with primary antibody diluted in a blocking solution. The anti-LUM(sc-166871, Santa Cruz Biotechnology; dilution 1:50) and secondary peroxidase-conjugated antibodies were used. Sections were counterstained with hematoxylin and examined under a Nikon Eclipse 80i microscope. The histochemical staining level of LUM blocks was evaluated by two experienced clinical pathologists with blind testing. Data were analyzed using Image J software, and the positive and highly positive areas were included in the statistical analysis.

2.10. Statistical analysis

Statistical analyses were performed using GraphPad Prism 8.0 (GraphPad Software, Inc) and are presented as mean ± SD. For two-group comparisons, the unpaired *t*-test was used, while Welch's unequal variances *t*-test was applied when two normally distributed datasets had unequal variance. Survival analysis was carried out using the Kaplan-Meier method and compared using the log-rank test. Correlation analysis was conducted using Spearman's correlation. Levels of significance were indicated as follows: *p < 0.05; **p < 0.01; ***p < 0.001; ****p < 0.0001.

3. Results

3.1. Identification of DEGs and establishment of PPI network

In this study, two gene expression datasets, GSE56363 and GSE168009, were analyzed to identify differentially expressed genes (DEGs) in advanced stage cervical squamous cell carcinoma (CESC) patients after concomitant chemoradiotherapy (CCRT).

In GSE56363, 21 patients at advanced stage CESC were clinically evaluated at 6 months after the end of the concomitant CCRT, and were defined as complete response (CR, 12 patients) or non-complete response (NCR, 9 patients) (partial response and stable disease)

according to WHO efficacy evaluation standard RECIST1.1.753 DEGs, including 223 up-regulated DEGs and 386 down-regulated DEGs, were obtained in NCR patients compared with CR patients. In GSE168009, 4 patients with no durable benefit that progression-free period <3 years were defined as NDB group, 5 patients with durable clinical benefit that progression-free period >5 years were defined as DCB group according to the WHO efficacy evaluation standard RECIST1.1. We got 1065 DEGs, including 513 up-regulated DEGs and 552 down-regulated DEGs in NDB patients compared with DCB patients. Volcano plots were used to visualize the distribution of DEGs in both datasets (Fig. 1A). A Venn diagram was used to demonstrate the intersections of genes between the two datasets, revealing 86 co-differentially expressed genes (67 up-regulated and 19 down-regulated) (Fig. 1B). A PPI network of DEGs was constructed using the STRING database and visualized by the Cytoscape software (Fig. 1C). The top 10 hub genes, including COL6A3, ADAMTS2, COL1A1, MMP2, LUM, COL3A1, FBN1, COL6A1, COL5A1, and VCAN, were identified and used to construct subnetworks (Fig. 1D). GO analysis revealed that the top 10 DEGs are associated with endodermal cell differentiation and collagen fibril organization (Fig. 1E). To account for intratumor heterogeneity in gene expression profiles, the expression of these DEGs was examined in the RNA microarray data GSE5787, containing 33 biopsies from 11 patients. LUM was the only DEG with a statistically significant differential expression between NCR and CR patients (Fig. 1F).

3.2. Single-cell atlas of the tumor ecosystem in CESC

To investigate the potential role of LUM in the tumor microenvironment of CESC, single-cell RNA sequencing from GSE168652 was reanalyzed. This dataset comprises two samples, one from a tumor and one from adjacent normal tissue. After filtering out low-quality cells, 11,289 cells from the tumor sample and 9,649 cells from the adjacent normal sample remained for analysis. t-distributed stochastic neighbor embedding (t-SNE) was used to visualize the global distribution of cells (Fig. 2A–C). Both tumor and normal tissues exhibited heterogeneity, displaying a distinct distribution of cells with different origins (Fig. 2A). The cells were divided into seven main cell types based on differentially expressed genes in each cluster and cell-specific marker genes provided by the original study: epithelial cells, smooth muscle cells, fibroblasts, endothelial cells, endometrial stromal cells, lymphocytes, and macrophages (Fig. 2B).

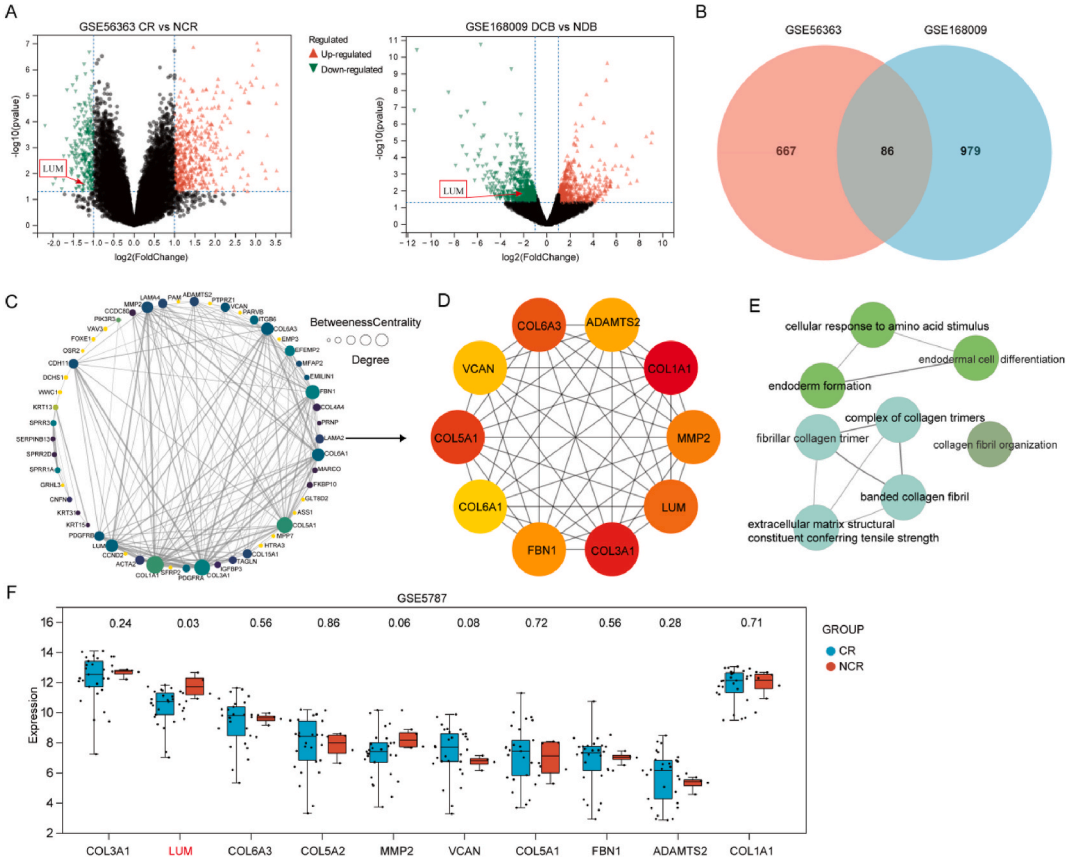

Fig. 1. Identification of DEGs. (A) Volcano plots show the differentially expressed genes identified from GSE56363 and GSE168009. The vertical lines represent Log2FC, and the horizontal lines represent a *p*-value of 0.05. (B) Venn diagram demonstrates the intersections of genes between GSE56363 and GSE168009. (C) PPI network of 86 DEGs. (D) PPI network of the top 10 hub genes. The gradual color represents the degree value. (E) GO enrichment analysis of the top 10 hub genes. (F) Boxplot shows the top 10 hub genes expression in the GSE5787 datasets. (For interpretation of the references to color in this figure legend, the reader is referred to the Web version of this article.)

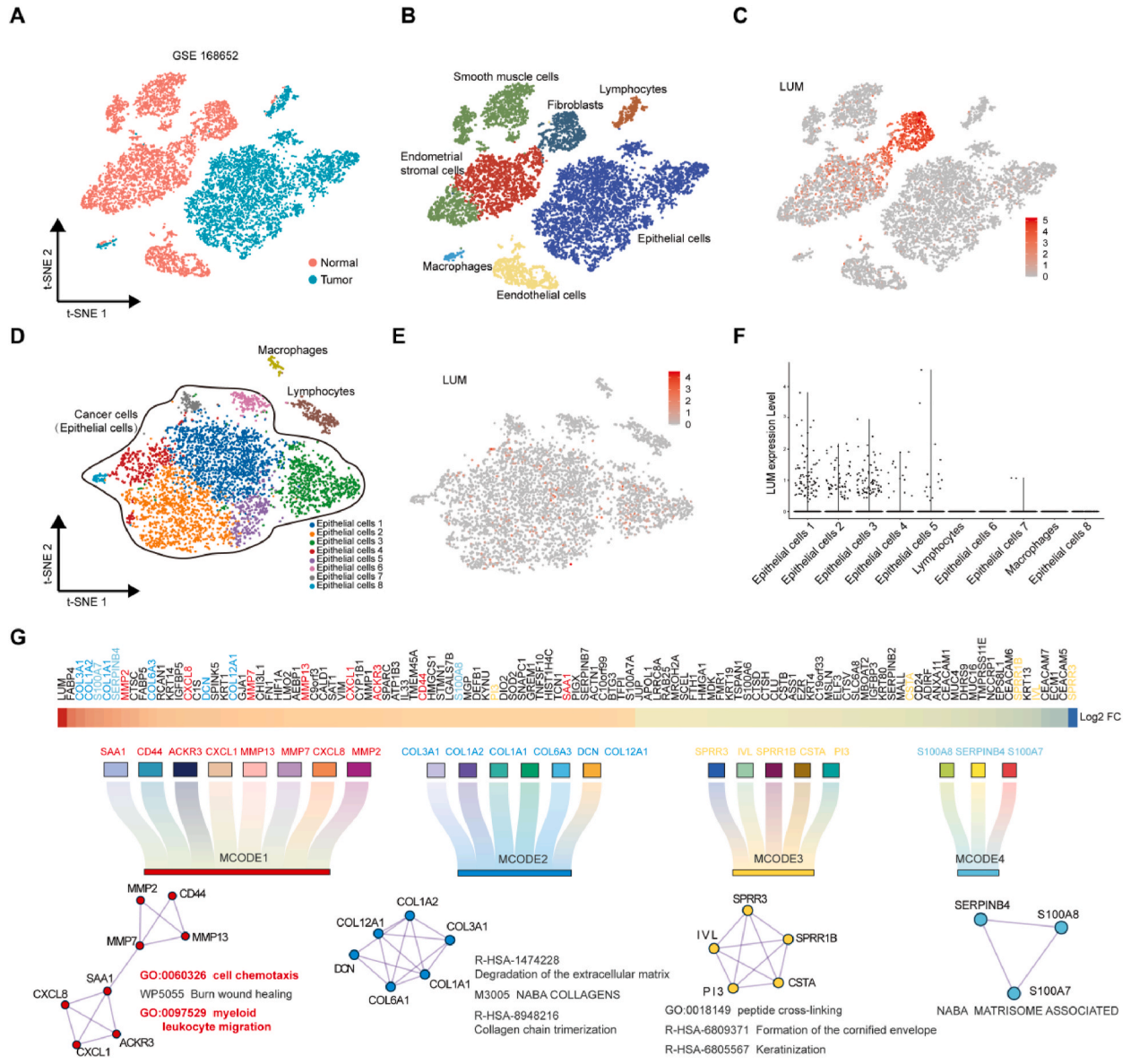

Fig. 2. Comprehensive cellular overview of the CESC ecosystem. (A) Single-Cell Transcriptome Analysis by t-SNE and single cells colored by tissue origin. (B) The t-SNE plot shows the different cell clusters. (C) The t-SNE plot shows LUM's expression in adjacent normal and cancer cells. (D) Defined cell types in tumor cells according to LUM expression. (E) The t-SNE plot shows the LUM expression in various cell types in the cancer group. (F) Violin plot shows the LUM expression across multiple cell types in the cancer group. (G) Heatmap of DEGs in LUM+ and LUM-tumor cells and the enrichment analysis of MCODEs.

LUM expression levels in different cell types were then displayed on the map, LUM was significantly higher in adjacent normal cells than cancer cells, especially in fibroblasts and endometrial stromal cells (Fig. 2C).

Unsupervised cluster analysis was used to define 8 distinct cell types based on LUM expression levels in tumor cells. LUM was rarely expressed in epithelial cells 6 and 8, as well as in lymphocytes and macrophages (Fig. 2D–F). The Gene Ontology Biological Process (GOBP) - Gene Set Variation Analysis (GSVA) score analysis of the clusters revealed that epithelial 6 and 8 exhibited higher metalloendopeptidase activity and downregulation of TGF-β stimulation (Supplementary Fig. 1). Tumor cells were further divided into LUM+ and LUM-groups to explore the differences in biological behavior between these two tumor molecular subtypes. The PPI network of DEGs were grouped into 4 major clusters using the MCODE method. Enrichment revealed significant regulation in cell chemotaxis and myeloid leukocyte migration in MCODE 1 (Fig. 2G).

3.3. Comparison of the cellular interaction between cancer cells and immune cells

To understand how multiple cell populations and signaling pathways function collectively, CellChat was used to explore cellular interaction in GSE168652. Tumor cells were divided into LUM+ and LUM-groups to investigate the communication between different groups of cancer cells and immune cells (Fig. 3A and B). LUM+ and LUM-cancer cells shared some common communication patterns with immune cells such as TNFSF12, SPP1, NAMPT, MIF, MDK, LGALS9, IFNG, HBEGF, ANGPTL4 and CCL5. In the CESC tumor microenvironment, macrophages and lymphocytes account for the majority of immune cells, we focused on the communication pattern between tumor cells and these two immune cells. IFNG was identified as a shared communication pattern between both LUM-

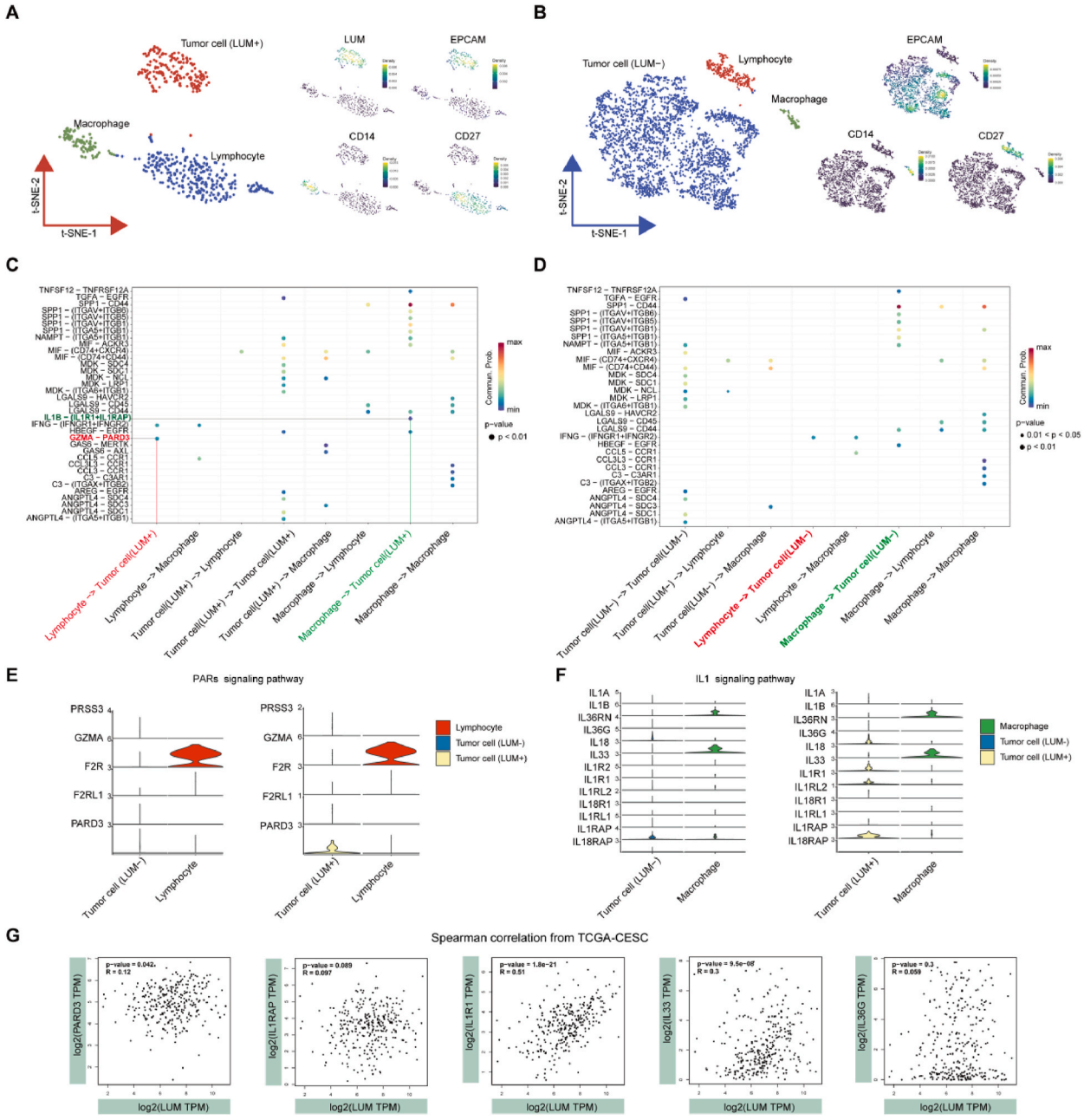

Fig. 3. Analysis of Cell-Cell Communication Network Using CellChat. (A) The t-SNE plot shows the LUM + expression in CESC cell types. (B) The t-SNE plot shows the LUM-expression in CESC cell types. (C) Communication patterns between LUM + CESC cells and lymphocytes and macrophages. (D) Communication patterns between LUM- CESC cells and lymphocytes and macrophages. (E) Violin plot demonstrates the expression of PARs signaling pathway in CESC cell and lymphocytes. (F) Violin plot exhibits the expression of IL1 signaling pathway in CESC cell and macrophages. (G) The relationship between LUM expression and PARs signaling pathway and IL1 signaling pathways in TIMER.

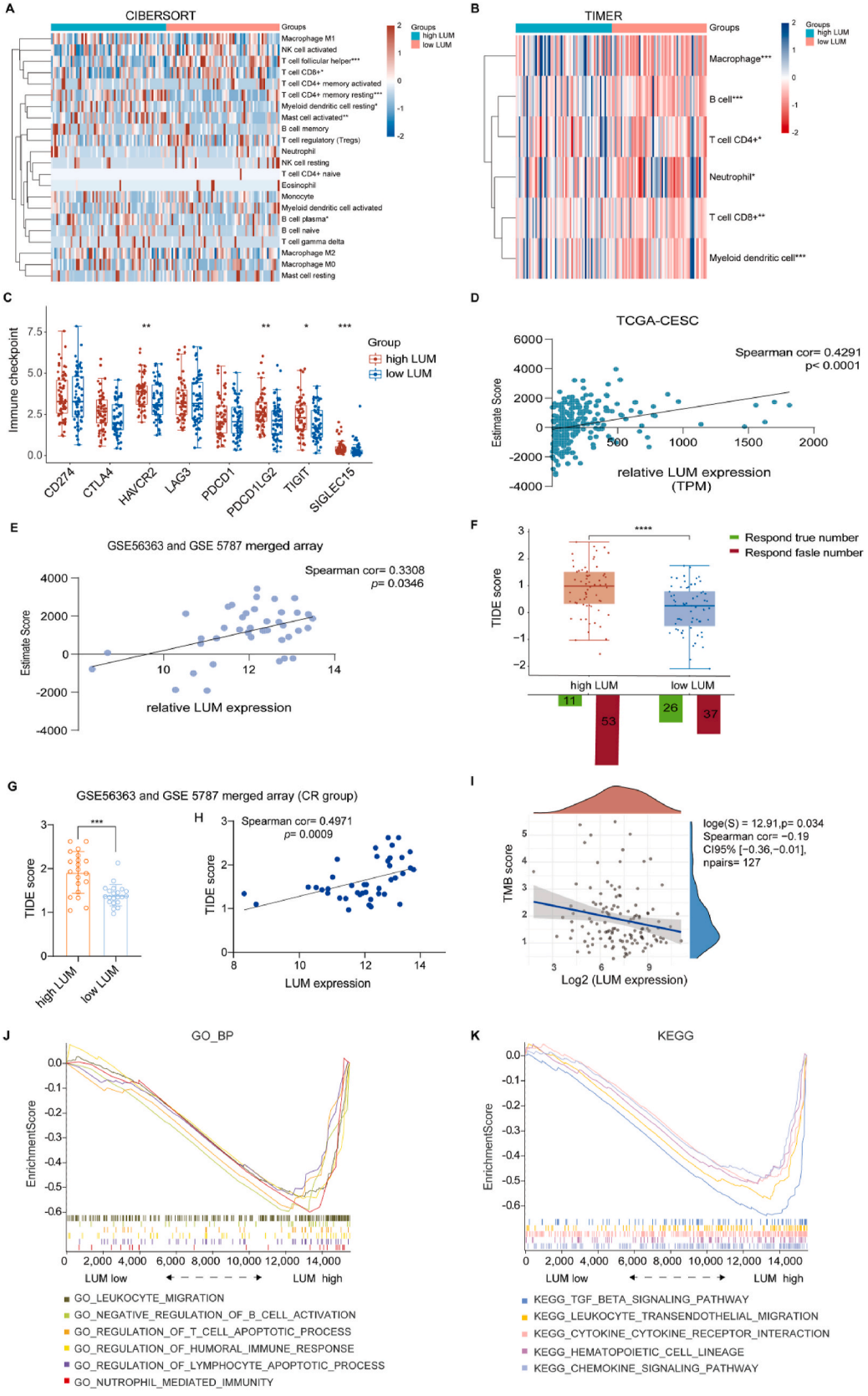

(caption on next page)

Fig. 4. Correlation of LUM expression with immune infiltration and immune checkpoint in CESC patients. (A) Heatmap shows 22 immune cell type proportions in TCGA-CESC samples estimated by CIBERSORT. (B) Heatmap displays that the TIMER algorithm estimated seven immune cell type proportions in TCGA-CESC samples. (C) Boxplot demonstrates immune checkpoints in the high (highest 25%) expression LUM group and the low (lowest 25%) expression LUM group in TCGA-CESC RNA-seq data. (D) The scatter plot depicts the Spearman correlation analysis of ESTIMATE scores and relative LUM expression in TCGA-CESC RNA-seq data. (E) The scatter plot depicts the Spearman correlation analysis of ESTIMATE scores and relative LUM expression in GSE56363 and GSE5787 merged data. (F) Clinical response rate of patients with high (highest 25%) expression LUM group and the low (lowest 25%) LUM group for CCRT in TCGA-CESC RNA-seq data. (G) Bar diagram shows the average TIDE scores of high and low LUM groups (highest 25% compared with lowest 25%) in GSE56363 and GSE5787 merged data. (H)The scatter plot depicts the Spearman correlation analysis of TIDE scores of high and low LUM groups (highest 25% compared with lowest 25%) in GSE56363 and GSE5787 merged data. (I) Correlation between the LUM expression and the TMB score in TCGA-CESC. (J) GO-BP for significant pathways of CESC-CR patients. (K) KEGG for significant pathways of CESC-CR patients. All data were presented as mean ± S.D. *$p < 0.05$; **$p < 0.01$; ***$p < 0.001$; ****$p < 0.0001$.

and LUM + CESC cells and lymphocytes. However, GZMA-PARD3 was a unique communication pattern between lymphocytes and LUM + CESC cells. IL1-B was an distinct communication pattern between macrophages and LUM + CESC cells (Fig. 3C and D). Differential communication network mediated by ligand-receptor interactions across all cellular components in the PARs signaling pathway and IL1 signaling pathway were then investigated. The violin plot showed a significant expression of F2R in lymphocytes, but PARD3 was only expressed in LUM + cell types and salient expression in LUM-cells (Fig. 3E). In the ligand-receptor interactions in the IL1 signaling pathway, the expression of IL1RAP and IL36G was much stronger in LUM + cell types than in LUM-cell types, IL1R1 and IL33 were found only in LUM + cell types (Fig. 3F). Inspired by the communication patterns results, the relationship between LUM expression and PARs signaling pathway and IL1 signaling pathways in TIMER was further analyzed. LUM was positively correlated with PARD3 ($p = 0.042$), IL1R1 ($p = 1.8e\text{-}21$), and IL33 ($p = 9.5e\text{-}08$). Compared with LUM- CESC cells, LUM + CESC cells are more active in communication with macrophages and lymphocytes.

3.4. Tumor immune infiltration predict response of CCRT in CESC

To explore the relationship between LUM and CESC immune microenvironment, the composition of 22 tumor-infiltrating immune cells was compared between high-LUM and low-LUM groups in TCGA-CESC using the CIBERSORT algorithm. The results indicated that the infiltration levels of T cell follicular helper and T cell $CD8^+$ were decreased in the high-LUM group, while T cell $CD4^+$ memory resting, myeloid dendritic cell resting, mast cell activated, and B cell plasma were increased in the high-LUM group (Fig. 4A). The TIMER database results also revealed a close correlation between LUM and immune cells (Fig. 4B). Moreover, the RNA expression of 8 immune checkpoints was further investigated in high and low LUM groups, HAVCR2, PDCD1LG2, TIGIT, and SIGLEC15 were highly expressed in the high (highest 25%) LUM groups compared with the low (lowest 25%) LUM groups (Fig. 4C). The TME score was calculated using the ESTIMATE algorithm in TCGA-CESC, the expression level of LUM was positively correlated with the ESTIMATE score ($p < 0.0001$) (Fig. 4D). Similar results were obtained in the analysis of the merged GSE56363 and GSE5787 array ($p = 0.0346$)

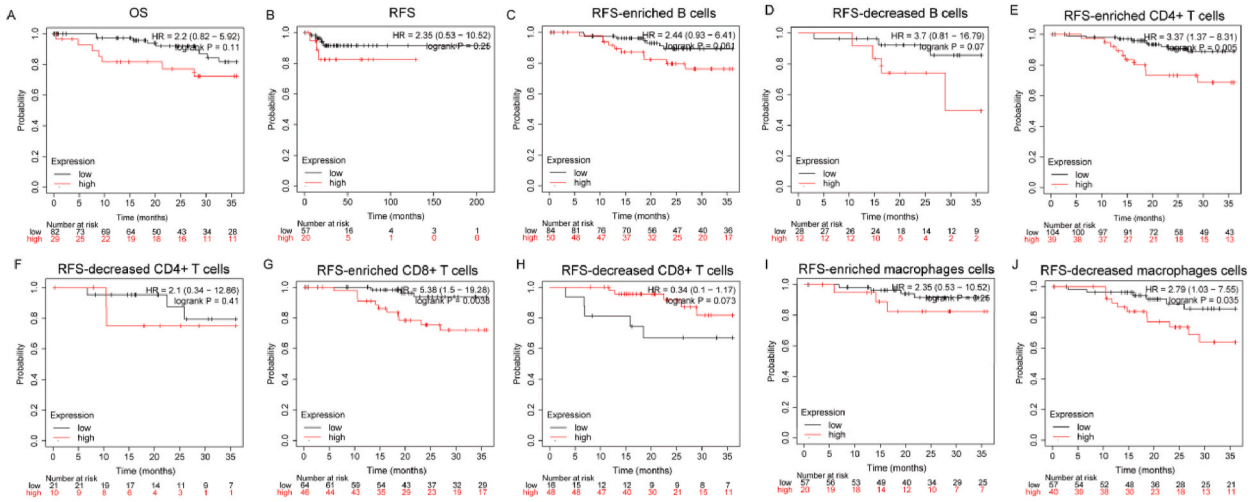

Fig. 5. Comparison of Kaplan-Meier curves of the high and low expression of LUM in TCGA-CESC. (A) OS of high and low expression of LUM in TCGA-CESC; (B) RFS of high and low expression of LUM in TCGA-CESC; (C) (C) RFS of high and low expression of LUM in enriched B cells cohort; (D) RFS of high and low expression of LUM in decreased B cells cohort; (E) RFS of high and low expression of LUM in enriched $CD4^+$ T cells cohort; (F) RFS of high and low expression of LUM in decreased $CD4^+$ T cells cohort; (G) RFS of high and low expression of LUM in enriched $CD8^+$ T cells cohort; (H) RFS of high and low expression of LUM in decreased $CD4^+$ T cells cohort; (I) RFS of high and low expression of LUM in enriched macrophages cells cohort; (J) RFS of high and low expression of LUM in decreased macrophages cells cohort.

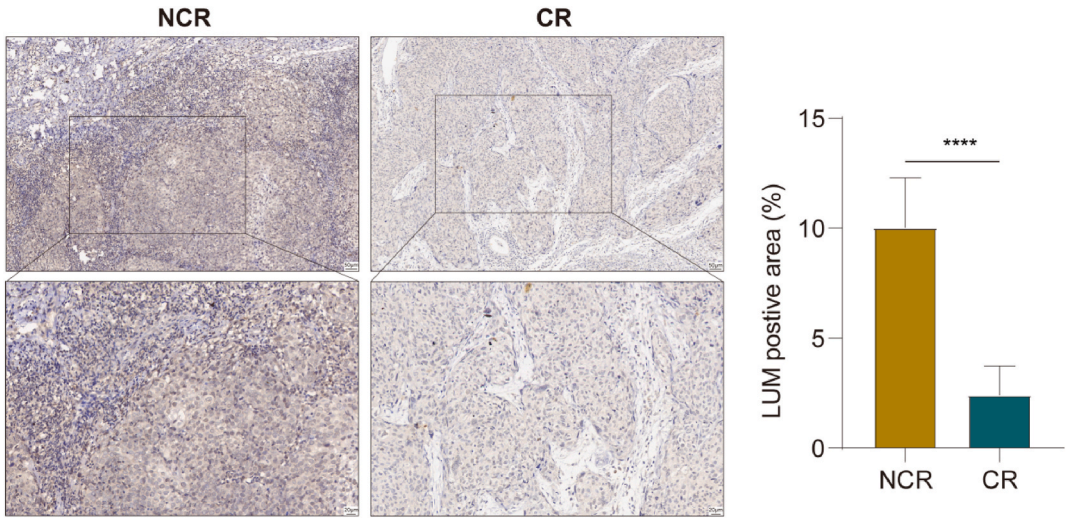

Fig. 6. Representative immunohistochemical staining of LUM in CR and NCR CESC tissues. and quantitative statistics. Left: NCR CESC tissues; Right: CR CESC tissues. The square frame indicate the region that is magnified in the insert (up: × 200; down: × 400). ****$p < 0.0001$.

(Fig. 4E). Since both chemotherapy and radiotherapy can affect the tumor immune microenvironment, TIDE and TMB are considered markers of the tumor immune microenvironment in multiple cancers [25–28]. In this study, LUM had a positive correlation with TIDE in TCGA-CESC, patients with high LUM had higher TIDE scores than patients with low LUM ($p < 0.001$), and the proportion of patients with true response to CCRT in the high-LUM group was also higher than that in the low-LUM group (high LUM: true: 18%, false: 82%; low LUM: true, 41%; false, 59%) (Fig. 4F). Additionally, TIDE was used to estimate the response to CCRT in GSE56363 and GSE5787. The results demonstrated that LUM was also significantly positively correlated with TIDE score (Pearson r = 0.47, $p = 0.0019$) (Fig. 4G and H), but the TMB score was negatively correlated with the LUM expression in TCGA-CESC RNA-seq data (Fig. 4I).

Overall, these results indicate that the LUM may be used as a predictor of tumor immune microenvironment and may predict the response to CCRT in CESC. The enrichment analysis in CR patients in GSE56363 and GS5787 suggested that low LUM CESC samples are associated with the activation of immune-related pathways according to the GO enrichment analysis (Fig. 4J). For instance, leukocyte migration, negative regulation of B cell activation, regulation of T cell apoptotic process, regulation of lymphocyte cell apoptotic process, regulation of humoral immune response, and neutrophil-mediated immunity are higher in low LUM CESC cells according to the GO enrichment analysis. Simultaneously, leukocyte transendothelial migration, cytokine-cytokine receptor interaction, and hematopoietic cell lineage. In the meantime, the TGF-BETA signaling pathway and chemokine signaling pathway are activated in low LUM CESC samples (Fig. 4K). Therefore, the immune landscape may be different between high and low LUM CESC samples, and it may contribute to the various clinical outcome to CCRT.

3.5. Prognostic analysis of LUM expressions in CESC based on immune cells

Having confirmed that the expression of LUM was correlated with immune infiltration in CESC, and possibly related to the treatment effect, we speculated that the expression of LUM might affect the treatment response partly because of immune infiltration in CESC. First, we performed a prognostic analysis using Kaplan-Meier plotter based on the expression levels of LUM in overall survival (OS) and relapse free survival (RFS) in CESC-TCGA. The results showed no significant correlation between the LUM expression and the OS ($p = 0.11$) (Fig. 5A) or RFS ($p = 0.26$) (Fig. 5B), indicating that LUM does not have prognostic value for survival in CESC. Next we conducted a prognosis analysis based on the expression levels of LUM in related immune cells subgroup using the Kaplan-Meier plotter. According to the RNA-seq expression of tumor tissues of patients in the TCGA-CESC database, the expression levels of LUM were grouped into the high-expression and low-expression groups based on the median value, and the follow-up threshold was 36 mouths. The results showed no significant correlation between the LUM and the RFS in the enriched and decreased B cells cohort (Fig. 5C and D). The low expression of LUM of CESC in enriched $CD4^+$ T cells and enriched $CD8^+$ T cells cohort had better RFS, respectively (Fig. 5E–H). Low expression of LUM in decreased macrophages cohort had better RFS, but there was no significant correlation between the LUM and the RFS in the enriched macrophages cells cohort (Fig. 5I and J). The above analysis suggested that low LUM expressions in CESC may affect prognoses in part due to T cell and macrophage cell immune infiltration.

3.6. Immunostaining of LUM in CESC tissue samples

The immunostaining of LUM in CESC tissue samples further supports the findings of our analysis. By dividing the 15 CESC patients into the CR group (7 patients) and NCR group (8 patients) based on the curative effect evaluation 6 months after CCRT. The expression

of LUM in the CR group was significantly lower than that in the non-CR group (Fig. 6). This observation is consistent with the previous results, indicating that low LUM expression may be associated with a better response to CCRT in CESC patients.

4. Discussion

This study aimed to explore genes related to CCRT resistance and their functional roles in CESC. Eventually, LUM was identified as a candidate gene for further investigation after integrated bioinformatics analysis.

LUM is a member of the small molecule proteoglycan family of leucine-rich repeats [29,30]. It is involved in cellular processes such as epithelial-mesenchymal transition, cell proliferation, migration, invasion, and adhesion [31–35]. Additionally, LUM is correlated with chemotherapy resistance in various tumors such as ovarian cancer, pancreatic cancer, and leukemia [36–38]. Yamano et al. [39] found LUM expression was significantly higher in cisplatin-resistant oral squamous cell carcinoma cell lines. Immunohistochemistry of tissue specimens from oral squamous carcinoma patients before receiving cisplatin-based neoadjuvant chemotherapy showed that LUM expression was higher in the chemo-resistant patients than in the chemo-responsive patients. Inhibition of LUM expression increased cisplatin-mediated apoptosis, suggesting that increased LUM expression was associated with cisplatin resistance in oral squamous carcinoma. Farace C et al. [40] found that glioblastoma and neuroblastoma stem cells have a time-dependent LUM expression in the stem cell environment. Stem cells with a high secretion of LUM are resistant to temozolomide at concentrations >750 μM, as evidenced by reduced apoptosis and increased cell viability. LUM plays a vital role in forming stem cell neurospheres and maintaining a quiescent stem cell-like phenotype, thereby affecting stem cell resistance to temozolomide. LUM's roles in the CESC are not well known, this study considers low LUM expression as a biomarker for predicting better CCRT response and survival prognosis in CESC patients.

LUM has multiple functions, including regulation of Fas-mediated immune activation [41]. Zang Y et al. [20] suggested that LUM can inhibit both immune escape and carcinogenic pathways in COAD. Based on the previous above studies on LUM and immune function, we hypothesize that LUM might influence the efficacy of CCRT by affecting tumor immunity capacity. In this study, we initially verified the association of LUM expression with CESC tumor cells using single-cell sequencing data. The molecular mechanism revealed that the expression of LUM is significantly positively associated with immune cell-related signaling pathways through GSEA. Previous studies have confirmed that radiotherapy and chemotherapy response were related to immune capacity, since the tumor immune microenvironment plays a critical role in cancer development and metastasis. Infiltration of various types of immune cells and stroma cells in tumor parenchyma might be a promising source of drug target and prognostic biomarker [42–44]. Tumor-infiltrating lymphocytes (TILs), essential components of the tumor microenvironment, are potential predictor of CCRT, providing crucial information such as treatment response and tumor behavior in various cancers, such as nasopharyngeal, lung, and cervical [45–47]. In this study, we explored the abundance of immune cells and stromal cells in the TME using the CIBERSOFT and TIMER, finding that high-LUM is related to increased infiltration of immune cells, specifically T lymphocytes and macrophages. Since immune-suppressive cells play an important role in abrogating the effectiveness of ICIs [48], we investigated the potential response of NDB and DCB patients to ICIs. TIDE is an algorithm for predicting ICB response based on gene expression profiles. A high TIDE score indicates that it is more likely to become a nonresponder for immunotherapy. Our results indicate that the TIDE score was positively correlated with the expression level of LUM, suggesting that high LUM expression has a high TIDE score. The failure rate to CCRT in the high LUM group was significantly higher than that in the low LUM expression group, indicating that high LUM expression CESC patients might have a worse response to immunotherapy than low LUM expression patients. TMB is also known to be a predictive marker for anti-PD-1 therapy [49], the results were similar between patients with high and low NDB scores. Although ICI therapy for CESC is the second or third-line treatment after failure of CCRT, this study assessed the effect of CCRT on the expression of immune cells in CESC patients, suggesting that individualized ICI therapy following CCRT treatment may improve CESC outcomes.

Previous studies had reported that increased infiltration of $CD8^+$ T cells into tumors is associated with progression in cancers like melanoma, and breast, greater $CD8^+$ T cell infiltration of tumors could predict response to standard chemotherapy and immune checkpoint blockade therapy, such as anti-CTLA-4 therapy or anti-PD-1 therapy [50,51]. Our results indicated that greater infiltration of enriched $CD4^+$ T cells and enriched $CD8^+$ T cells was correlated with better RFS in patients with CESC. However, compared to macrophages cells enriched patients, decreased infiltration of macrophages cells patients had RFS benefits. Therefore, measuring the extent of T cell and macrophage infiltration of CESC is crucial. Our GSEA analysis also demonstrated that most genes identified as closely related to immune cell infiltration by WGCNA were enriched in immunomodulatory activities, such as the T cell apoptotic process, regulation of lymphocyte cell apoptotic process, cytokine-cytokine receptor interaction, hematopoietic cell lineage, and chemokine signaling pathway.

IL1 pathways contribute significantly to stress response and inflammation. IL1B can promote tumor-promoting inflammation in breast cancer, and it can be targeted in metastatic breast cancer patients with a soluble IL1 receptor antagonist, and also can be an immunomodulatory target in treatment-resistant breast cancer [52]. IL1 pathway is strongly induced by irradiation and correlate with radioresistance and senescence, especially IL1A and IL1B which exhibit excellent associations [53]. Our cell-cell communication network identified a strong association of the IL1 pathway with the macrophages, suggesting that the IL1 pathway might be involved in CESC CCRT resistance. PAR-induced cellular signaling may be activated through G-protein interaction or arrestin association, depending on the receptor type, the activation of PARs increases the transcription of cytokines and chemokines to suppression of antitumor immunity [54,55]. In this study, PAR-2 was the special subtype specificity expressed in LUM + cell types and generates signal communication with lymphocytes.

In conclusion, this study initially reported the function of the LUM gene in CESC with CCRT. Low LUM expression was positively correlated with good response to CCRT and prognosis in CESC patients. LUM could be a promising and predictive prognostic biomarker

in CESC, and might serve as a potential target for personalized therapy in CESC patients treated with CCRT. However, the study has limitations, as the function of LUM and downstream signaling affecting CCRT response requires further investigation based on more experiments.

Author contribution statement

Ge Hu, Ying Xiao and Chanchan Ma: Performed the experiments; Analyzed and interpreted the data; Wrote the paper.
Jinyun Wang, Xiaotao Qian, Xiaowei Wu and Fengqin Zhu: Contributed reagents, materials, analysis tools or data.
Junchao Qian and Shiying Sun: Conceived and designed the experiments.

Data availability statement

Data included in article/supp. material/referenced in article.

Declaration of competing interest

The authors declare that they have no known competing financial interests or personal relationships that could have appeared to influence the work reported in this paper.

Acknowledgements

This work was supported by the National Natural Science Foundation of China (grant number U1932158, 81871085 and 82271519), Natural Science Foundation of Shandong Province (grant number ZR2019LZL018), Anhui Province Funds for Distinguished Young Scientists (grant number 2208085J10), Collaborative Innovation Program of Hefei Science Center, CAS (grant number 2019HSC-CIP003), China Postdoctoral Science Foundation (grant number 2019M652403), Project of Postdoctoral Innovation of Shandong Province (grant number 202002048).

Appendix A. Supplementary data

Supplementary data to this article can be found online at https://doi.org/10.1016/j.heliyon.2023.e18011.

References

[1] A. Gradissimo, J. Lam, J.D. Attonito, J. Palefsky, L.S. Massad, X. Xie, I.E. Eltoum, L. Rahangdale, M.A. Fischl, K. Anastos, H. Minkoff, X. Xue, G. D'Souza, L. C. Flowers, C. Colie, S. Shrestha, N.A. Hessol, H.D. Strickler, R.D. Burk, Methylation of high-risk human papillomavirus genomes are associated with cervical precancer in HIV-positive women, Cancer Epidemiol. Biomarkers Prev. 27 (2018) 1407–1415.
[2] J.M. Lemp, J.W. De Neve, H. Bussmann, S. Chen, J. Manne-Goehler, M. Theilmann, M.E. Marcus, C. Ebert, C. Probst, L. Tsabedze-Sibanyoni, L. Sturua, J. M. Kibachio, S.S. Moghaddam, J.S. Martins, D. Houinato, C. Houehanou, M.S. Gurung, G. Gathecha, F. Farzadfar, S. Dryden-Peterson, J.I. Davies, R. Atun, S. Vollmer, T. Barnighausen, P. Geldsetzer, Lifetime prevalence of cervical cancer screening in 55 low- and middle-income countries, JAMA 324 (2020) 1532–1542.
[3] D. Viveros-Carreno, A. Fernandes, R. Pareja, Updates on cervical cancer prevention, Int. J. Gynecol. Cancer 33 (2023) 394–402.
[4] Y. Liu, Y. Xu, W. Jiang, H. Ji, Z.W. Wang, X. Zhu, Discovery of key genes as novel biomarkers specifically associated with HPV-negative cervical cancer, Mol. Ther. Meth. Clin. Dev. 21 (2021) 492–506.
[5] D. Nguyen, K.T. Simms, A. Keane, G. Mola, J.W. Bolnga, J. Kuk, P.J. Toliman, S.G. Badman, M. Saville, J. Kaldor, A. Vallely, K. Canfell, Towards the elimination of cervical cancer in low-income and lower-middle-income countries: modelled evaluation of the effectiveness and cost-effectiveness of point-of-care HPV self-collected screening and treatment in Papua New Guinea, BMJ Glob. Health 7 (2022).
[6] A. Keane, J.F. Shi, K.T. Simms, Y.J. Liu, J.B. Lew, C. Mazariego, S. Yuill, R.F. Wu, Z.H. Liu, F.H. Zhao, J. Jeronimo, K. Canfell, Y.L. Qiao, Health economic evaluation of primary human papillomavirus screening in urban populations in China, Canc. Epidemiol. 70 (2021), 101861.
[7] M. Guo, J. Xu, J. Du, Trends in cervical cancer mortality in China from 1989 to 2018: an age-period-cohort study and Joinpoint analysis, BMC Publ. Health 21 (2021) 1329.
[8] L. Li, Y. Gong, K. Xu, W. Chen, J. Xia, Z. Cheng, L. Li, R. Yu, J. Mu, X. Le, Q. Xiang, W. Peng, J. Tang, T. Xiang, ZBTB28 induces autophagy by regulation of FIP200 and Bcl-XL facilitating cervical cancer cell apoptosis, J. Exp. Clin. Cancer Res. 40 (2021) 150.
[9] F. Qin, H. Pang, T. Yu, Y. Luo, Y. Dong, Treatment strategies and prognostic factors of 2018 FIGO stage IIIC cervical cancer: a review, Technol. Cancer Res. Treat. 21 (2022), 2081139005.
[10] J. Fu, W. Wang, Y. Wang, C. Liu, P. Wang, The role of squamous cell carcinoma antigen (SCC Ag) in outcome prediction after concurrent chemoradiotherapy and treatment decisions for patients with cervical cancer, Radiat. Oncol. 14 (2019) 146.
[11] H. Lu, Y. Wu, X. Liu, H. Huang, H. Jiang, C. Zhu, Y. Man, Z. Chen, X. Long, Q. Pang, L. Peng, X. Li, J. Gu, S. Deng, L. Xing, Endostar, an antiangiogenesis inhibitor, combined with chemoradiotherapy for locally advanced cervical cancer, Oncol. Res. 28 (2022) 929–944.
[12] C. Beskow, A.K. Agren-Cronqvist, F. Granath, B. Frankendal, R. Lewensohn, Pathologic complete remission after preoperative intracavitary radiotherapy of cervical cancer stage Ib and IIa is a strong prognostic factor for long-term survival: analysis of the Radiumhemmet data 1989-1991, Int. J. Gynecol. Cancer 12 (2002) 158–170.
[13] G.A. Taarnhoj, I.J. Christensen, H. Lajer, K. Fuglsang, M.M. Jeppesen, H.S. Kahr, C. Hogdall, Risk of recurrence, prognosis, and follow-up for Danish women with cervical cancer in 2005-2013: a national cohort study, Canc. Am. Canc. SOC 124 (2018) 943–951.
[14] T. Shu, D. Zhao, B. Li, Y. Wang, S. Liu, P. Li, J. Zuo, P. Bai, R. Zhang, L. Wu, Prognostic evaluation of postoperative adjuvant therapy for operable cervical cancer: 10 years' experience of National Cancer Center in China, Chin. J. Cancer Res. 29 (2017) 510–520.

[15] C. Liu, Y. Hu, Z. Wang, H. Pan, Y. Ren, X. Li, Z. Liu, H. Gao, The downregulation of placental lumican promotes the progression of preeclampsia, Reprod. Sci. 28 (2021) 3147–3154.
[16] Y.S. Lee, S.J. Park, J.Y. Lee, E. Choi, B.J. Kim, Benefits of lumican on human bone health: clinical evidence using bone marrow aspirates, Korean J. Intern. Med. (Korean Ed.) 37 (2022) 821–829.
[17] N. Matsushima, H. Miyashita, R.H. Kretsinger, Sequence features, structure, ligand interaction, and diseases in small leucine rich repeat proteoglycans, J. Cell Commun. Signal 15 (2021) 519–531.
[18] J. Zappia, M. Joiret, C. Sanchez, C. Lambert, L. Geris, M. Muller, Y. Henrotin, From translation to protein degradation as mechanisms for regulating biological functions: a review on the slrp family in skeletal tissues, Biomolecules 10 (2020).
[19] N. Yamauchi, Y. Kanke, K. Saito, H. Okayama, S. Yamada, S. Nakajima, E. Endo, K. Kase, L. Yamada, H. Nakano, T. Matsumoto, H. Hanayama, Y. Watanabe, S. Hayase, M. Saito, Z. Saze, K. Mimura, T. Momma, S. Oki, Y. Hashimoto, K. Kono, Stromal expression of cancer-associated fibroblast-related molecules, versican and lumican, is strongly associated with worse relapse-free and overall survival times in patients with esophageal squamous cell carcinoma, Oncol. Lett. 21 (2021) 445.
[20] Y. Zang, Q. Dong, Y. Lu, K. Dong, R. Wang, Z. Liang, Lumican inhibits immune escape and carcinogenic pathways in colorectal adenocarcinoma, Aging (Albany NY) 13 (2021) 4388–4408.
[21] X. Li, D. Roife, Y. Kang, B. Dai, M. Pratt, J.B. Fleming, Extracellular lumican augments cytotoxicity of chemotherapy in pancreatic ductal adenocarcinoma cells via autophagy inhibition, Oncogene 35 (2016) 4881–4890.
[22] P. Nizet, V. Untereiner, G.D. Sockalingum, I. Proult, C. Terryn, A. Jeanne, L. Nannan, C. Boulagnon-Rombi, C. Sellier, R. Rivet, L. Ramont, S. Brezillon, Assessment of ovarian tumor growth in wild-type and lumican-deficient mice: insights using infrared spectral imaging, Histopath. Immunohistochem. Canc. 13 (2021).
[23] S. Appunni, M. Rubens, V. Ramamoorthy, V. Anand, M. Khandelwal, A. Saxena, P. McGranaghan, Y. Odia, R. Kotecha, A. Sharma, Lumican, pro-tumorigenic or anti-tumorigenic: a conundrum, Clin. Chim. Acta 514 (2021) 1–7.
[24] K.C. Hsiao, P.Y. Chu, G.C. Chang, K.J. Liu, Elevated expression of lumican in lung cancer cells promotes bone metastasis through an autocrine regulatory mechanism, Cancers 12 (2020).
[25] S. Zhu, Y. Wang, J. Tang, M. Cao, Radiotherapy induced immunogenic cell death by remodeling tumor immune microenvironment, Front. Immunol. 13 (2022), 1074477.
[26] J. Zhang, M. Yang, X. Fan, M. Zhu, Y. Yin, H. Li, J. Chen, S. Qin, H. Zhang, K. Zhang, F. Yu, Biomimetic radiosensitizers unlock radiogenetics for local interstitial radiotherapy to activate systematic immune responses and resist tumor metastasis, J. Nanobiotechnol. 20 (2022) 103.
[27] J. Lin, Y. Cai, Y. Ma, J. Pan, Z. Wang, J. Zhang, Y. Liu, Z. Zhao, A new signature that predicts progression-free survival of clear cell renal cell carcinoma with anti-PD-1 therapy, Int. J. Mol. Sci. 24 (2023).
[28] C. Uruena, P. Lasso, D. Bernal-Estevez, D. Rubio, A.J. Salazar, M. Olaya, A. Barreto, M. Tawil, L. Torregrosa, S. Fiorentino, The breast cancer immune microenvironment is modified by neoadjuvant chemotherapy, Sci. Rep. 12 (2022) 7981.
[29] K. Karamanou, M. Franchi, I. Proult, R. Rivet, D. Vynios, S. Brezillon, Lumican inhibits in vivo melanoma metastasis by altering matrix-effectors and invadopodia markers, Cells-Basel 10 (2021).
[30] H.J. Cho, Y.S. Lee, D.A. Kim, S.A. Moon, S.E. Lee, S.H. Lee, J.M. Koh, Lumican, an exerkine, protects against skeletal muscle loss, Int. J. Mol. Sci. 23 (2022).
[31] X. Li, M.A. Truty, Y. Kang, X. Chopin-Laly, R. Zhang, D. Roife, D. Chatterjee, E. Lin, R.M. Thomas, H. Wang, M.H. Katz, J.B. Fleming, Extracellular lumican inhibits pancreatic cancer cell growth and is associated with prolonged survival after surgery, Clin. Cancer Res. 20 (2014) 6529–6540.
[32] C.T. Yang, J.M. Li, W.K. Chu, S.E. Chow, Downregulation of lumican accelerates lung cancer cell invasion through p120 catenin, Cell Death Dis. 9 (2018) 414.
[33] K. Karamanou, M. Franchi, Z. Piperigkou, C. Perreau, F.X. Maquart, D.H. Vynios, S. Brezillon, Lumican effectively regulates the estrogen receptors-associated functional properties of breast cancer cells, expression of matrix effectors and epithelial-to-mesenchymal transition, Sci. Rep. 7 (2017), 45138.
[34] X. Li, Y. Kang, D. Roife, Y. Lee, M. Pratt, M.R. Perez, B. Dai, E.J. Koay, J.B. Fleming, Prolonged exposure to extracellular lumican restrains pancreatic adenocarcinoma growth, Oncogene 36 (2017) 5432–5438.
[35] K.E. Williams, L.A. Fulford, A.R. Albig, Lumican reduces tumor growth via induction of fas-mediated endothelial cell apoptosis, Canc. Microenviron. 4 (2010) 115–126.
[36] Z. Yu, L. Liu, Q. Shu, D. Li, R. Wang, Leukemia stem cells promote chemoresistance by inducing downregulation of lumican in mesenchymal stem cells, Oncol. Lett. 18 (2019) 4317–4327.
[37] K.R. Abou, K. Brodaczewska, A. Filipiak, N.A. Zeinelabdin, S. Buart, C. Szczylik, C. Kieda, S. Chouaib, Tumor hypoxia regulates immune escape/invasion: influence on angiogenesis and potential impact of hypoxic biomarkers on cancer therapies, Front. Immunol. 11 (2020), 613114.
[38] K. Wilkinson, W. Ng, T.L. Roberts, T.M. Becker, S.H. Lim, W. Chua, C.S. Lee, Tumour immune microenvironment biomarkers predicting cytotoxic chemotherapy efficacy in colorectal cancer, J. Clin. Pathol. 74 (2021) 625–634.
[39] Y. Yamano, K. Uzawa, K. Saito, D. Nakashima, A. Kasamatsu, H. Koike, Y. Kouzu, K. Shinozuka, K. Nakatani, K. Negoro, S. Fujita, H. Tanzawa, Identification of cisplatin-resistance related genes in head and neck squamous cell carcinoma, Int. J. Cancer 126 (2010) 437–449.
[40] C. Farace, J.A. Oliver, C. Melguizo, P. Alvarez, P. Bandiera, A.R. Rama, G. Malaguarnera, R. Ortiz, R. Madeddu, J. Prados, Microenvironmental modulation of decorin and lumican in temozolomide-resistant glioblastoma and neuroblastoma cancer stem-like cells, PLoS One 10 (2015), e134111.
[41] F. Wu, N. Vij, L. Roberts, S. Lopez-Briones, S. Joyce, S. Chakravarti, A novel role of the lumican core protein in bacterial lipopolysaccharide-induced innate immune response, J. Biol. Chem. 282 (2007) 26409–26417.
[42] S. Cheng, E.J. Cheadle, T.M. Illidge, Understanding the effects of radiotherapy on the tumour immune microenvironment to identify potential prognostic and predictive biomarkers of radiotherapy response, Cancers 12 (2020).
[43] A. Prasetyo, J. Budiman, U. Sadhana, The relationship between tumor-infiltrating lymphocytes (TILs) and nasopharyngeal carcinoma (NPC): a systematic review, Iran J. Otorhinolary. 33 (2021) 191–200.
[44] K. Yoneda, T. Kuwata, M. Kanayama, M. Mori, T. Kawanami, K. Yatera, T. Ohguri, M. Hisaoka, T. Nakayama, F. Tanaka, Alteration in tumoural PD-L1 expression and stromal CD8-positive tumour-infiltrating lymphocytes after concurrent chemo-radiotherapy for non-small cell lung cancer, Br. J. Cancer 121 (2019) 490–496.
[45] I.F. van Luijk, S.M. Smith, O.M. Marte, A.L. Oei, G.G. Kenter, E.S. Jordanova, A review of the effects of cervical cancer standard treatment on immune parameters in peripheral blood, tumor draining lymph nodes, and local tumor microenvironment, J. Clin. Med. 11 (2022).
[46] M. Datta, L.M. Coussens, H. Nishikawa, F.S. Hodi, R.K. Jain, Reprogramming the tumor microenvironment to improve immunotherapy: emerging strategies and combination therapies, Am Soc Clin Oncol Educ Book 39 (2019) 165–174.
[47] D. Sha, Z. Jin, J. Budczies, K. Kluck, A. Stenzinger, F.A. Sinicrope, Tumor mutational burden as a predictive biomarker in solid tumors, Cancer Discov. 10 (2020) 1808–1825.
[48] R.A. Leon-Letelier, D.I. Castro-Medina, O. Badillo-Godinez, A. Tepale-Segura, E. Huanosta-Murillo, C. Aguilar-Flores, S.G. De Leon-Rodriguez, A. Mantilla, E. M. Fuentes-Panana, C. Lopez-Macias, L.C. Bonifaz, Induction of progenitor exhausted tissue-resident memory CD8(+) T cells upon Salmonella typhi porins adjuvant immunization correlates with melanoma control and anti-PD-1 immunotherapy cooperation, Front. Immunol. 11 (2020), 583382.
[49] K. Wu, X. Zheng, Z. Yao, Z. Zheng, W. Huang, X. Mu, F. Sun, Z. Liu, J. Zheng, Accumulation of CD45RO+CD8+ T cells is a diagnostic and prognostic biomarker for clear cell renal cell carcinoma, Aging (Albany NY) 13 (2021) 14304–14321.
[50] C.A. Egelston, C. Avalos, T.Y. Tu, D.L. Simons, G. Jimenez, J.Y. Jung, L. Melstrom, K. Margolin, J.H. Yim, L. Kruper, J. Mortimer, P.P. Lee, Human breast tumor-infiltrating CD8(+) T cells retain polyfunctionality despite PD-1 expression, Nat. Commun. 9 (2018) 4297.
[51] X. Zhou, Y. Ni, X. Liang, Y. Lin, B. An, X. He, X. Zhao, Mechanisms of tumor resistance to immune checkpoint blockade and combination strategies to overcome resistance, Front. Immunol. 13 (2022), 915094.
[52] T.C. Wu, K. Xu, J. Martinek, R.R. Young, R. Banchereau, J. George, J. Turner, K.I. Kim, S. Zurawski, X. Wang, D. Blankenship, H.M. Brookes, F. Marches, G. Obermoser, E. Lavecchio, M.K. Levin, S. Bae, C.H. Chung, J.L. Smith, A.M. Cepika, K.L. Oxley, G.J. Snipes, J. Banchereau, V. Pascual, J. O'Shaughnessy, A.

K. Palucka, IL1 receptor antagonist controls transcriptional signature of inflammation in patients with metastatic breast cancer, Cancer Res. 78 (2018) 5243–5258.

[53] D.K. Tiwari, R. Hannen, K. Unger, S. Kohl, J. Hess, K. Lauber, F. Subtil, E. Dikomey, R. Engenhart-Cabillic, U. Schotz, IL1 pathway in HPV-negative HNSCC cells is an indicator of radioresistance after photon and carbon ion irradiation without functional involvement, Front. Oncol. 12 (2022), 878675.

[54] Y. Yang, A. Stang, P.G. Schweickert, N.A. Lanman, E.N. Paul, B.P. Monia, A.S. Revenko, J.S. Palumbo, E.S. Mullins, B.D. Elzey, E.M. Janssen, S.F. Konieczny, M. J. Flick, Thrombin signaling promotes pancreatic adenocarcinoma through PAR-1-dependent immune evasion, Cancer Res. 79 (2019) 3417–3430.

[55] X. Liu, J. Yu, S. Song, X. Yue, Q. Li, Protease-activated receptor-1 (PAR-1): a promising molecular target for cancer, Oncotarget 8 (2017) 107334–107345.